Microchimica Acta (2022) 189: 154
https://doi.org/10.1007/s00604-022-05220-w

ORIGINAL PAPER

A universal strategy of glyconanoparticle preparation using a bifunctional linker for lectin sensing and cell imaging

Qiuyue Sha[1] · Jian Fei[1] · Chang Tu[1] · Bi-Feng Liu[1] · Zhaoyu Hu[1] · Xin Liu[1]

Received: 25 October 2021 / Accepted: 5 February 2022 / Published online: 25 March 2022

Abstract

Glyconanoparticles (G-NPs), biofunctional nanomaterials that can fully combine the unique properties of nanoparticles (NPs) with the bioactivities of carbohydrates, have become an appealing nanoplatform in analytical chemistry and biomedical research. However, there is currently a lack of an efficient and universal method for facile immobilization of reducing carbohydrates on NPs while maintaining their structure integrity, greatly limiting the preparation and application of G-NPs. Herein, a new and universal strategy for preparing carbohydrate-functionalized gold nanoclusters (Au NCs) was developed by using S-(3-(methoxyamino)propyl) thioacetate (MPTA) as a new bifunctional linker. MPTA with an N-methoxyamine group (-NHOMe) and a thioacetyl group (-SAc) was synthesized by a two-step strategy and then grafted onto Au NCs by an efficient click reaction. Subsequently, reducing carbohydrates could be readily immobilized onto MPTA-functionalized Au NCs (MPTA-Au NCs) by a reducing end ring-closure reaction under mild conditions. The obtained G-NPs showed average size of 1.9 ± 0.42 nm and strong fluorescence at 610 nm. Carbohydrates grafted on G-NPs still retained their structure integrity and specific recognition ability toward their receptor proteins. Notably, the affinity between G-NPs and proteins was increased by 1300 times compared with free carbohydrates with an association constant of $(1.47 \pm 0.356) \times 10^6\ M^{-1}$. The prepared fluorescent G-NPs were also successfully applied to lectin sensing and targeted breast cancer cell imaging with good performance. These results indicated that the intact immobilization of reducing carbohydrates (whether naturally or chemically accessed) on NPs could be easily achieved using MPTA, providing a simple, efficient, and universal strategy for G-NP preparation.

Keywords Glyconanoparticles · N-Alkylmethoxyamine · Reducing end ring-closure reaction · Lectin sensing · Cell imaging

Introduction

Carbohydrate-mediated interactions with proteins and other molecules are extensively responsible for many normal and pathogenic cellular activities in biological systems [1–3]. Therefore, studying and applying the carbohydrate-based interactions are of great significance for the development of new therapeutic and diagnostic strategies for human diseases [4, 5]. In order to overcome the limitation of weak binding affinity based on individual carbohydrate and to better investigate the carbohydrate-based interactions, NPs with large specific surface areas are selected as great scaffolds for loading carbohydrate ligands to mimic the glycoconjugates presenting on cell surface and to achieve higher binding affinity by multivalency effect [6–9]. The perfect combination of NPs' unique properties and carbohydrates' biological activities makes G-NPs an appealing nanoplatform

Qiuyue Sha and Jian Fei contributed equally to this work.

✉ Zhaoyu Hu
huzhaoyu@126.com

✉ Xin Liu
xliu@mail.hust.edu.cn

[1] Britton Chance Center for Biomedical Photonics at Wuhan National Laboratory for Optoelectronics – Hubei Bioinformatics & Molecular Imaging Key Laboratory, Systems Biology Theme, Department of Biomedical Engineering, College of Life Science and Technology, Huazhong University of Science and Technology, Wuhan 430074, China

for analytical chemistry and biomedicine research, such as carbohydrate-based biosensing, bioimaging, drug delivery, antiadhesive therapy, vaccine preparation, and targeted cancer therapy [10–15]. Notably, as a new-emerged class of gold nanomaterials, Au NCs consisting of several to hundreds of gold atoms exhibit more intriguing properties, such as super-small size, good monodispersity, and remarkable fluorescence with tunable wavelength, nontoxicity, and good biocompatibility [16–18]. The unique properties of Au NCs make them promising multivalent scaffolds for loading carbohydrate ligands. However, Au NC-based G-NPs have rarely been reported and one important limitation is the lack of an efficient and universal method for G-NP preparation especially for the crucial step—immobilization of carbohydrates on NPs [13].

In general, there are mainly two methods to perform this crucial step: non-covalent attachment and covalent attachment [14, 19]. Non-covalent attachment such as electrostatic interactions, hydrogen bonding, van der Waals forces, and hydrophobic interactions often shows poor stability and low specificity, thus leading to the increasing of non-specific adsorption and severely reducing the sensitivity and selectivity when applied to biomedical fields [14]. In contrast, covalent attachment exhibiting better stability and specificity is more frequently used for the immobilization of carbohydrates on NPs [14, 19]. During the past two decades, various covalent approaches have been explored for the immobilization of carbohydrates on NPs, such as amide coupling, reductive amination, and click chemistry [20]. The covalent methods either require tedious and time-consuming carbohydrate pre-derivatization to introduce appropriate functional groups at the reducing end for those synthetic carbohydrate or apply direct derivatization reactions of reducing carbohydrates for those natural or synthetic reducing carbohydrates. However, most of the current derivatization methods applied result ring-opened glycoconjugates, leading to the loss of carbohydrates' original biorecognition capabilities [13, 14, 21, 22]. Due to the above limitations, the existing carbohydrate-based nanosystem is relatively monotonous for the choice of carbohydrates. Many natural reducing oligosaccharides with important biological significance are often difficult to be used for G-NP construction and their further biomedical applications, such as tumor targeting therapy or vaccine development, are also difficult to realize. Therefore, there is an urgent need to develop a simple, efficient method for immobilizing reducing carbohydrates on NPs.

The perfluorophenylazide (PFPA)-based photoinitiated coupling method seemed to be a fast and simple method for immobilization of natural carbohydrates on NPs [23–25]. However, the insertion reaction based on PFPAs is not a single-point coupling and multiple linkers could insert into one carbohydrate molecule, which may result in net formation or molecular configuration change, further leading to epitope masking or activity loss of glycans in some case for those more complex system [26]. Otherwise, the N-methoxyamine functional group–based derivatization provides a single-point ring-closed coupling reaction toward reducing end of carbohydrate and linkers containing an N-methoxyamine group were applied for the preparation of glycoconjugates [22, 27–30]. The conjugation between this kind of linkers and carbohydrates shows excellent yield, stability toward hydrolytic cleavage, and great versatility, providing a potential promising strategy for G-NP preparation of reducing carbohydrates. However, the application of these linkers for G-NP preparation was not yet reported and the structure of the reported linkers could also be optimized especially on the terminal group for conjugation to nanoparticles.

In this work, a bifunctional linker MPTA containing an N-methoxyamine group and a thioacetyl group was firstly synthesized and introduced for covalently immobilizing carbohydrates onto Au NCs. A variety of reducing carbohydrates were immobilized on Au NCs using MPTA as a linker to evaluate the feasibility and versatility of this strategy for G-NP preparation. Taking mannose as an example, the loading amount of carbohydrates was evaluated by a classical sulfuric acid-phenol colorimetric method. The fluorescence response of lectin receptors to the as-prepared G-NPs was investigated to verify the activity of carbohydrates on G-NPs. In addition, the affinity between G-NPs and their corresponding lectin receptor was determined by isothermal titration calorimetry (ITC). The applications of the as-prepared G-NPs in lectin sensing and cancer cell imaging were also investigated in detail.

Experimental

Chemicals and reagents

The materials and reagents in this work were in analytical-reagent grade and used directly without further purification. Chloroauric acid hydrated ($HAuCl_4 \cdot 4H_2O$) was purchased from Chemical Reagent Co., Ltd. of Shanghai (Shanghai, China). L-Glutathione reduced (GSH), methoxylamine hydrochloride, sodium cyanoborohydride, sodium acetate an-hydrous, dichloromethane, ethanol, hydroxylamine hydro-chloride ($NH_2OH \cdot HCl$), D-mannose (Man), D-glucose (Glu), D-lactose monohydrate (Lac), monosialoganglioside (GM3), and phenol were obtained from Yinuokai Technology Co., Ltd. (Beijing, China). 4-Maleimidobutyric acid N-hydroxysuccinimide ester (GMBS), acrolein, L-fucose (Fuc), and 4-aminophenyl α-D-mannopyranoside (NH_2-Man) were provided by Aladdin Industrial Corporation (Shanghai, China). Thioacetic acid and concanavalin A (Con A) were obtained from Sigma Aldrich (St. Louis, MO, USA). The cell counting kit-8 (CCK-8) was purchased from

Dojindo Laboratories (Kyushu, Japan). The human breast cancer MDA-MB-231 cells and Swiss albino 3T3 cells were purchased from Procell Life Technology Co., Ltd. (Wuhan, China). The ultrapure water (18.2 MΩ) used in this work was generated by a Milli-Q device (Millipore, MA, USA).

Characterization

The UV-vis spectra were recorded on a Lambda 950 UV/Vis/NIR spectrophotometer (PerkinElmer, USA). The fluorescence spectra were measured on a QE 6500 fluorescence spectrometer (Ocean Optics, USA). Time-correlated single photo counting and the measurement of absolute fluorescence quantum yield were performed on an FLS 980 series of fluorescence spectrometers (Edinburgh, UK). High-resolution transmission electron microscopy (HR-TEM) images were recorded using a Tecnai G2 F30 transmission electron microscope (FEI, Holland) under an accelerating voltage of 300 kV. ^{1}H and ^{13}C NMR spectra were recorded on a Bruker Avance III 600 spectrometer at 600 MHz using $CDCl_3$ as solvent. The chemical shifts were given in δ values (ppm), using tetramethylsilane (TMS) as the internal standard; coupling constants (J) were given in Hz. The signal multiplicities were described as s (singlet), d (doublet), t (triplet), q (quartet), m (multiplet), and br (broad signal). Fourier transform infrared spectra (FT-IR) were measured on a Nicolet 5700 FT-IR spectrometer (Thermo Fisher Scientific, USA). The HR-MS were determined by a two-dimensional liquid chromatography-ion trap mass spectrometry. Isothermal titration calorimetry (ITC) experiments were performed using an ITC200 Microcalorimeter from MicroCal, LLC (Northampton, MA), in phosphate buffer (PBS). The concentration of lectin was 10 μM, and that of the G-NPs was 0.6 mg/mL. In each individual experiment, 38 μL of G-NPs was injected through the computer-controlled 40 μL microsyringe at an interval of 2 min into the lectin solution in the same buffer (cell volume = 200 μL) while stirring at 1000 rpm. The experimental data were fitted to a theoretical titration curve using the software supplied by MicroCal. The fluorescence images of two kinds of cells were observed on an FV3000 laser scanning confocal microscopy (Olympus, Japan).

General procedures for the preparation of carbohydrate-conjugated fluorescent Au NCs

Glutathione-stabilized gold nanoclusters (GSH-Au NCs) were prepared according to a previously described method [31]. Briefly, freshly prepared aqueous solutions of $HAuCl_4$ (20 mM, 9 mL) and GSH (100 mM, 2.7 mL) were mixed with 78.3 mL of ultrapure water at room temperature for 15 min. Then, the reaction mixture was gently stirred at 70 °C for 24 h. After the reaction, the mixture turned to yellow and displayed strong orange fluorescence under UV radiation, indicating the formation of GSH-Au NCs. The Au NC solution was purified by an ultrafiltration device (Millipore, USA) with a molecular weight cutoff of 3000 Da and stored in the dark at 4 °C before use.

For the coupling of MPTA to GSH-Au NCs, a bifunctional crosslinker GMBS containing a maleimide group and a succinimide ester group was firstly introduced onto GSH-Au NCs as follows: 4 mL of GSH-Au aqueous solution was dispersed in 6 mL of PBS (10 mM, pH 7.2~7.4). Then, 5 mg of GMBS dissolved in DMSO was dropped into the above solution. The reaction mixture was stirred for 8~10 h at room temperature. The obtained GMBS-Au NCs were purified by an ultrafiltration device with a molecular weight cutoff of 3000 Da.

For the grafting of MPTA onto GMBS-Au NCs, the aqueous solution of GMBS-Au NCs was firstly dispersed in 6 mL of PBS (0.1 M, pH 6.0). Then, 11 mg of MPTA dissolved in DMSO was dropped into the above solution, followed by the rapid addition of 64 mg $NH_2OH{\cdot}HCl$. The reaction mixture was stirred for 3 h at room temperature. The obtained MPTA-Au NCs was purified by an ultrafiltration device with a molecular weight cutoff of 3000 Da.

The general procedure for chemical ligation of reducing carbohydrates with MPTA-Au NCs was as follows: MPTA-Au NC aqueous solution was dispersed in 6 mL of AcOH/NaOAc buffer (2 M, freshly prepared, pH 4.5). Then, desired amount of any nature monosaccharide or oligosaccharide was added and the reaction mixture was stirred for 24 h at room temperature [27]. The obtained Man-Au NCs were also purified by an ultrafiltration device with a molecular weight cutoff of 3000 Da to remove the unreacted carbohydrates and other small molecules.

Determination of carbohydrate density

Before determining the carbohydrate density, the carbohydrate concentration on the surface of Au NCs was evaluated by sulfuric acid-phenol method. Briefly, a freshly prepared aqueous phenol solution (6%, w/w) was added into a series of mannose aqueous solutions at different concentrations, followed by the slow addition of concentrated sulfuric acid in an ice bath. After being mixed well, the mixture was incubated at 40 °C for 30 min. The absorbance of the solution at 490 nm was measured by UV-visible spectrophotometer and the data were plotted against the concentration of mannose to obtain a linear regression equation. After being treated by phenol/sulfuric acid as described above, the carbohydrate concentration on the surface of Au NCs was calculated according to the standard equation. Then, the carbohydrate density was obtained according to the measured carbohydrate concentration and the structural formula of GSH-Au

Scheme 1 Synthesis scheme of compound a and MPTA

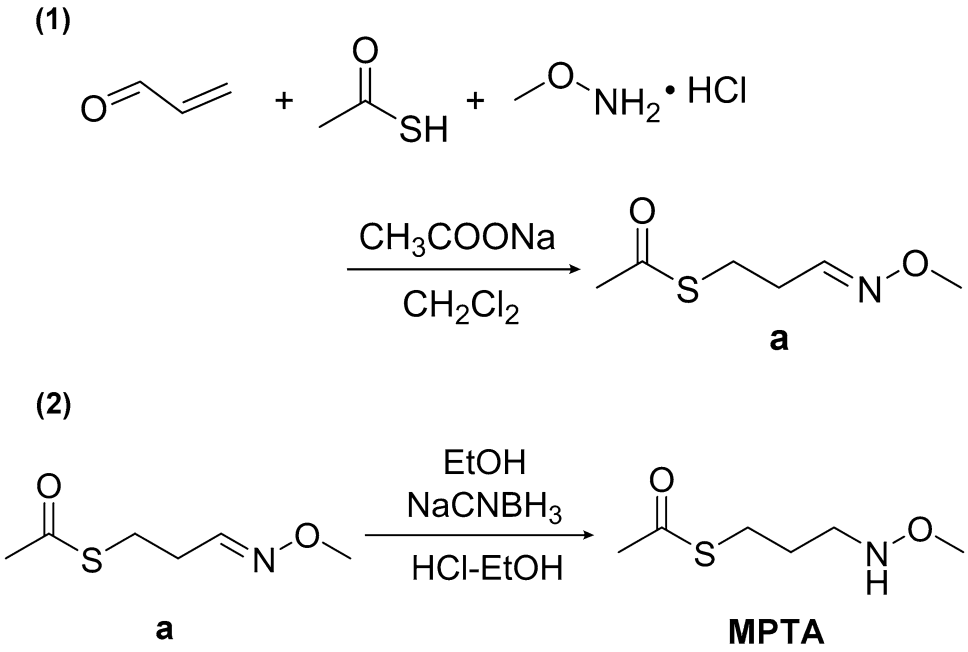

NCs reported by Xie's group [31]. The final data were the mean value of 3 measurements with less than 5% variation.

Lectin binding assay

Taking mannose as an example, the binding affinity of G-NPs with lectins was evaluated as the following procedure. PBS (pH 7.0, 10 mM, 0.1 mM Ca^{2+}, 0.1 mM Mn^{2+}) was employed as the binding buffer throughout the experiment. A total of 500 µL of Con A solution at different concentrations was added into 200 µL of diluted Man-Au NCs. After shaking for 30 min at 37 °C, the fluorescence intensity of each sample was tested with a fluorescence spectrometer. In the control group, Con A solution was added into GSH-Au NCs and treated as above.

Cell cytotoxicity and fluorescence imaging

Two cell lines were used for the cell imaging experiments: MDA-MB-231 and 3T3. All cell lines were cultured in high-glucose Dulbecco's modified Eagle's (DMEM) medium, which was supplemented with penicillin (100 µg mL^{-1}), streptomycin (100 µg mL^{-1}), and 10% fetal bovine serum (37 °C, 5% CO_2). The cell cytotoxicity assay was performed using CCK-8 assay. In brief, in the duration of propagation, cells were seeded in 96-well plates and cultured for 24 h, followed by the incubation with various concentrations of Man-Au NCs for 24 h. Subsequently, the medium was removed and 90 µL fresh medium and 10 µL CCK-8 solutions were added to each well with another 2-h incubation at 37 °C. Finally, the cell viabilities were calculated according to the absorption at 450 nm. For fluorescence cell imaging, the cells were seeded onto a 35 mm confocal dish and incubated at 37 °C for 48 h. After discarding the medium, cells were incubated with 300 µL of PBS (10 mM, pH 7.4), GSH-Au NCs, and Man-Au NCs respectively for 1.5 h at 37 °C in a 5% CO_2 incubator. After that, the cells were washed with PBS (10 mM, pH 7.4) for three times and imaged with an FV3000 confocal microscopy (Ex: 405 nm, Em: 550–650 nm).

Results and discussion

Synthesis and characterization of MPTA

In previous report, a thiol-containing N-alkylmethoxyamine was synthesized by Munneke et al. via a three-step method [27]. However, the conjugation of the N-alkylmethoxyamine did not lead to the desired glycosylamine and instead gave a diastereomeric mixture of thioaminals, which were formed via the nucleophilic attack of the thiol onto the oxime intermediate according to Munneke's report. Therefore, in our work, a thioacetyl group-contained oxyamine linker MPTA was designed and synthesized. Compared with Munneke's work, the original thiol group was protected with an acetyl group in MPTA, which not only avoided the attack of the thiol group toward the oxime intermediate while coupling with carbohydrates, but also facilitated the purification process and prevented it from being oxidized to disulfide during storage. The synthesis of MPTA took two steps as shown in Scheme 1. The detailed synthesis procedure of MPTA has been presented in "Electronic Supplementary Material." The first step involved the reaction of thioacetic acid, acrolein,

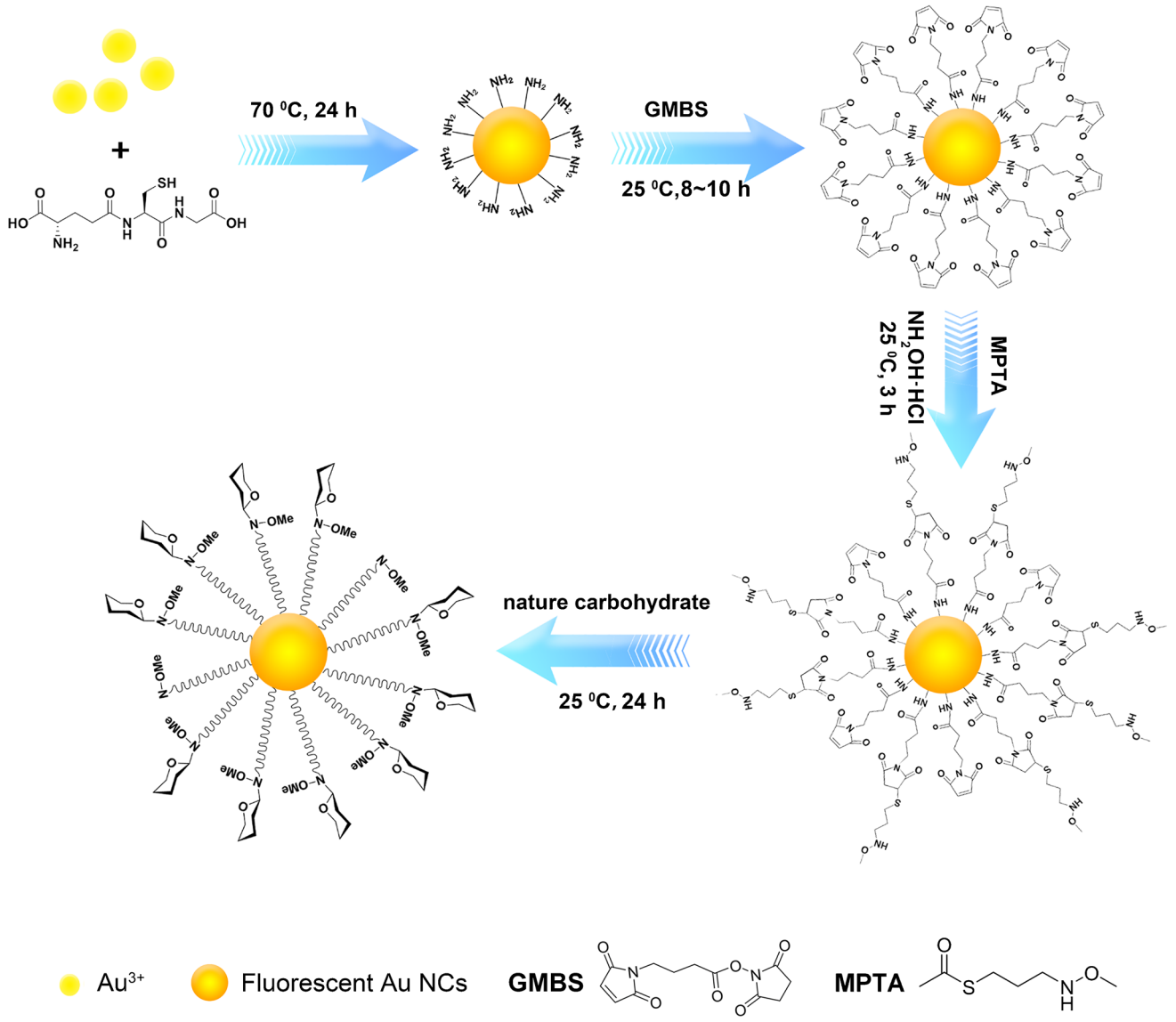

Scheme 2 Schematic diagram of the synthetic procedures of carbohydrate-functionalized GSH-Au NCs

and methoxylamine hydrochloride, leading to in situ thiolene reaction and oxime formation. The oxime was subsequently reduced by $NaCNBH_3$ in the second step, leading to the successful synthesis of MPTA. The structure verification of compound a and MPTA by NMR and HR-MS was presented in Fig. S1-6. More detailed result's discussion on the NMR and HR-MS spectra has been presented in "Electronic Supplementary Material."

Preparation and characterization of carbohydrate-conjugated GSH-Au NCs

Based on MPTA, carbohydrate-conjugated GSH-Au NCs were prepared easily on 4 steps (Scheme 2). Firstly, fluorescent GSH-Au NCs with aggregation-induced emission (AIE) property were firstly prepared using a natural tripeptide GSH as the model thiolate ligand according to the previous report [31]. As shown in Fig. 1a, the GSH-Au NCs were monodispersed in a spherical shape with an average diameter of 1.4 ± 0.15 nm. The solution of GSH-Au NCs was faint yellow in color under visible light and emitted an intense orange fluorescence under UV exposure (inset of Fig. 1c). The prepared GSH-Au NC solution displayed strong emission at 610 nm when excited at 427 nm as shown in Fig. 1c. The UV-vis absorption spectrum of GSH-Au NCs showed an onset at 500 nm and a shoulder peak at ~400 nm (Fig. 1c). Notably, none of surface plasma resonance at 520 nm was detected, excluding the formation of larger Au NPs. The oxidation state of Au in GSH-Au NCs was examined by X-ray photoelectron spectroscopy. As shown in Fig. S7, the

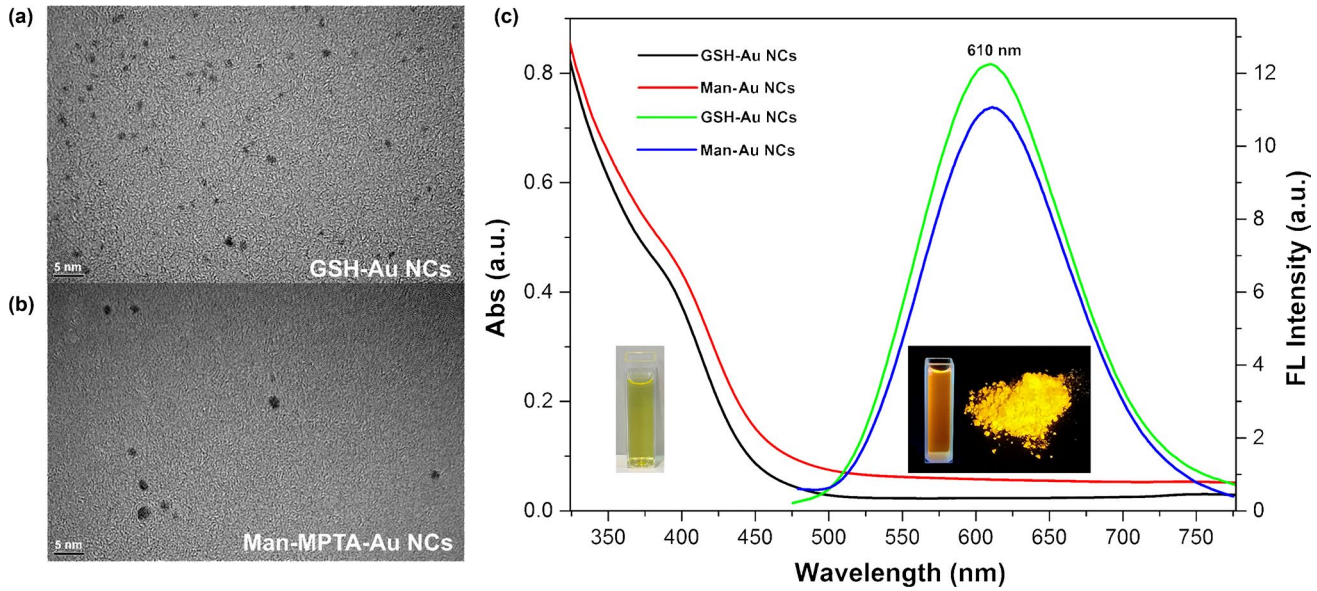

Fig. 1 HR-TEM images of **a** GSH-Au NCs and **b** Man-Au NCs; **c** UV-vis absorption spectra and fluorescence emission spectra of GSH-Au NCs and Man-Au NCs. Inset from left to right: images of GSH-Au NCs solutions under visible light and UV irradiation, respectively (the solid powder in the inner illustration is the freeze-dried powder of GSH-Au NCs)

Au 4f spectrum of GSH-Au NCs with the measured binding energy of 83.7 eV and 84.6 eV could be assigned to Au^0 and Au^+ respectively, confirming the (Au^0@Au^+-S) core-shell structure of GSH-Au NCs [31]. The average fluorescence lifetime of GSH-Au NCs in water was determined to be 8.142 ± 1.127 μs (Fig. S8). The absolute fluorescence quantum yield of GSH-Au NCs was determined to be 4.64%. Besides, GSH-Au NCs showed an average hydrodynamic size of 93.2 ± 12.1 nm, which may be attributed to the presence of a high content of compact aggregates of Au^+-S complexes in the shell of the core-shell nanostructure of GSH-Au NCs (Fig. S9) [31]. As the isoelectric point of GSH in the shell of GSH-Au NCs was far less than 7.4, the potential of GSH-Au NCs dispersed in phosphate buffer (pH 7.4) was −13.2 ± 1.8 mV as shown in Fig. S10. Furthermore, the hydrodynamic particle size and zeta potential of GSH-Au NCs in phosphate buffer (pH 7.4) remained stable within 80 h, indicating the good stability of GSH-Au NCs (Fig. S11). In a word, the as-prepared GSH-Au NCs presented excellent physicochemical properties, making them promising scaffolds for the construction of G-NPs. Secondly, maleimide groups were introduced on the surface of GSH-Au NCs by the reaction between the succinimide ester group of GMBS and the amino group of GSH. As shown in Fig. S12a, the strong peak at ~1644 cm^{-1} was derived from the stretching vibration of C=O on the amide bond of GSH. After GMBS modification, a new peak at 697 cm^{-1} occurred in Fig. S12b, which was assigned to the C-H bending vibration of -CH=CH-, suggesting the successful modification of GMBS. Thirdly, MPTA was induced onto GSH-Au NCs by the click reaction between thioacetyl group of MPTA and maleimide group of GMBS-GSH-Au NCs under the reduction of NH_2OH·HCl. As shown in Fig. S12C, the peak at 697 cm^{-1} disappeared after coupling with MPTA, indicating the successful addition reaction between MPTA and GMBS-GSH-Au NCs. Finally, reducing carbohydrates were easily immobilized on Au NCs by the ring-closure reaction between N-methoxyamine group of MPTA on Au NCs and aldehyde group of reducing carbohydrates. Taking mannose as an example, as shown in Fig. S12d, the enhanced peak at ~3387 cm^{-1} corresponded to the stretching vibrations of carbohydrates' hydroxyl groups, proving the successful preparation of carbohydrate-conjugated GSH-Au NCs.

In order to further investigate the feasibility of immobilizing carbohydrates on GSH-Au NCs by MPTA, taking mannose as an example, the changes in particle size and fluorescence properties of GSH-Au NCs before and after carbohydrate modification as well as the loading amount of carbohydrates were studied in detail. As shown in Fig. 1b, Man-Au NCs still appeared as monodisperse particles with an average size of 1.9 ± 0.42 nm, which was a little larger than that of GSH-Au NCs. Dynamic light scattering measurements (DLS) further verified the result, in which GSH-Au NCs showed an hydrodynamic size of 93 nm, while the hydrodynamic size of Man-Au NCs was at about 105 nm (Fig. S13). Compared to GSH-Au NCs, the fluorescence intensity of Man-Au NCs changed a little and the fluorescence emission wavelength remained unchanged (Fig. 1c), which indicated that the series of modifications did not brought too much adverse effect on the properties

of Au NCs. Besides, the loading amount of mannose on GSH-Au NCs was evaluated by a classical sulfuric acid-phenol colorimetric method. Mannose at different concentrations was treated with phenol-sulfuric acid solution, followed by the measurement of the absorbance at 490 nm to obtain a standard curve equation between the concentration of mannose and the absorbance as shown in Fig. S14 [32]. Man-Au NCs were then subjected to the same assay and the absorptions at 490 nm were recorded. As shown in Fig. S15a, Man-Au NCs diluted 10 times exhibited a 2.7 times stronger absorbance than that of GSH-Au NCs at 490 nm, proving the efficient immobilization of mannose on GSH-Au NCs by MPTA. The amount of mannose attached to Au NCs was subsequently derived from the calibration curve in Fig. S14b, which averaged at 98.22 ± 4.1 μg/mg Au NCs, corresponding to about 7~11 mannose per Au NCs (calculated according to the molecular formula of GSH-Au NCs reported by Xie's group) [31].

In addition to mannose, other reducing carbohydrates, including monosaccharides (glucose, galactose, and fucose) and oligosaccharides (lactose and GM3, a tumor-associated carbohydrate antigen), were also immobilized to GSH-Au NCs using MPTA as a linker. The resulting carbohydrate-Au NCs were subsequently treated with phenol-sulfuric acid solution and the UV-vis spectra were recorded. As shown in Fig. S15b, all carbohydrate-Au NCs showed apparent absorption at 490 nm, suggesting the successful modification of carbohydrates on GSH-Au NCs. These results further confirmed the versatility and high efficiency of this strategy for G-NP preparation from reducing carbohydrates.

Lectin binding assay by the as-prepared G-NPs

To further validate whether the formed G-NPs by this new strategy is suitable for biomedical applications, taking mannose as an example, their protein binding affinities, lectin sensing, and cancer cell imaging properties were investigated. Firstly, the lectin recognition capability of carbohydrates modified on GSH-Au NCs was studied by measuring the fluorescence response of receptor lectin to the as-prepared G-NPs. As shown in Fig. 2, the fluorescence intensity of Man-Au NCs was enhanced after the addition of Con A (a lectin that can specifically recognize D-mannose). While in the control group of GSH-Au NCs + Con A, no significant fluorescence enhancement was observed (Fig. S16). TEM analysis of Man-Au NCs in the presence of Con A (0.5 μM) showed that the originally monodispersed Man-Au NCs had a certain degree of aggregation as shown in Fig. 2a. Considering that the GSH-Au NCs prepared in this work exhibited AIE property, it could be inferred that the specific interaction between Con A and mannose on the surface of GSH-Au NCs caused the aggregation of Man-Au NCs, thus leading to the aggregation-induced fluorescence enhancement. To further confirm this hypothesis, DLS was also employed to investigate the change of hydrodynamic diameter of Man-Au NCs in the presence of Con A. As shown in Fig. S17, the hydrodynamic particle size of Man-Au NCs was about 105 nm in the absence of Con A. While after the addition of 0.5 μM of Con A, the hydrodynamic particle size of Man-Au NCs was greatly increased, which was consistent with the results observed by TEM. Based on the above findings, Man-Au NCs were further applied to the quantitative sensing of Con A. As shown in the inset of Fig. 2b, with the

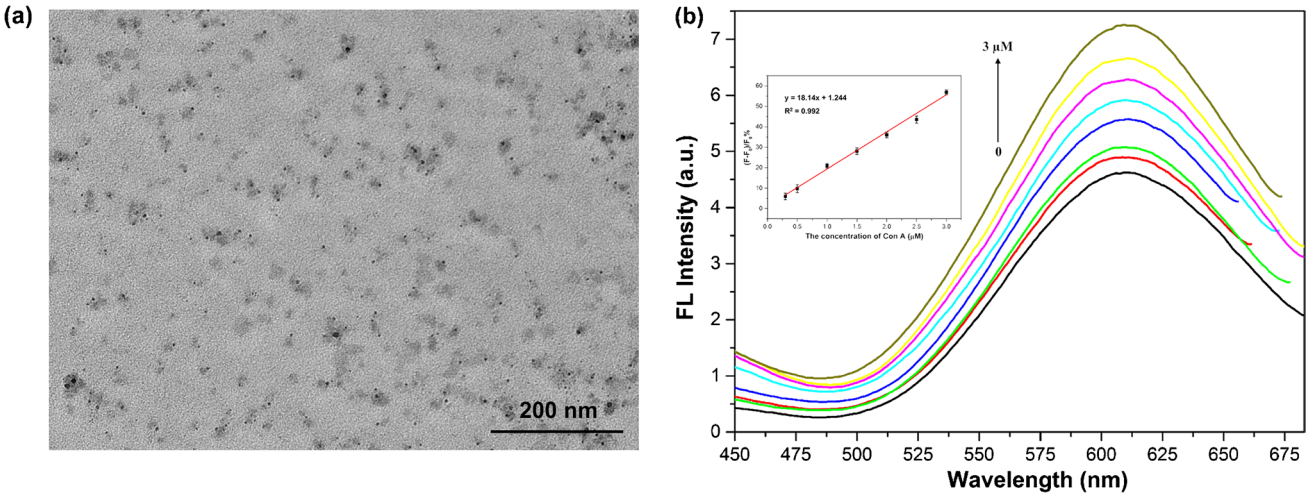

Fig. 2 **a** TEM image of Man-Au NCs in the presence of 0.5 μM of Con A; **b** fluorescence emission spectra of Man-Au NCs in the presence of different concentrations of Con A (0~3 μM). Inset: calibration curve between the percentage of fluorescence enhancement $(F-F_0)/F_0\%$ and the concentration of Con A over the range of 0.3–3 μM. F_0 and F were the fluorescence intensity of Man-Au NCs in the absence and presence of Con A, respectively. The error bars represented the standard deviation of three parallel tests

increasing concentration of Con A, the fluorescence intensity of MPTA-GSH-Au NCs gradually increased. There is a good linear relationship between the fluorescence enhancement percentage $(F - F_0)/F_0\%$ and the concentration of Con A over the range of 0.3 μM–3 μM, and the linear equation is $y = 18.14x - 1.244$ with a correlation coefficient (R^2) of 0.992 (inset of Fig. 2b). This result indicated that mannose modified on the surface of GSH-Au NCs still maintained its original biological activity and the as-prepared G-NPs by this strategy is suitable for lectin sensing.

Direct measurement of the affinity between G-NPs and lectin by ITC

To investigate whether the as-prepared G-NPs significantly enhance carbohydrates' binding affinity toward their receptors by multivalent effect due to carbohydrates' cluster presentation on NPs. The interaction between the as-prepared G-NPs and lectin was further quantitatively characterized by ITC according to method reported [9]. In the approach previously reported by our group, due to the lack of suitable method for reducing carbohydrate immobilization and the very limited options of available functionalized carbohydrate on the market, expensive functional mannose (4-aminophenyl α-D-mannopyranoside, NH_2-Man) had to be used to construct G-NPs for biosensing and bioimaging [32]. For comparison with the strategy developed in this work, the NH_2-Man-GSH-Au NCs was also prepared from NH_2-Man according to the method reported in our previous work.

In the ITC experiments, the binding affinity between free mannose and Con A was too weak to be detected (Fig. 3a), while obvious heat release was detected when Con A was titrated into the NH_2-Man-Au NCs solution, suggesting a stronger binding than free mannose as shown in Fig. 3b. For Man-Au NCs, each injection of the G-NP solution gave rise to a remarkable exothermic response and the heat release decreased gradually with each additional injection, yielding a typical titration isotherm (Fig. 3c). As a control, ITC experiments were performed with GSH-Au NCs/Con A in identical fashion. As shown in Fig. S18, the heat release was much less and remained essentially constant with each injection, which showed that no binding occurred between GSH-Au NCs and Con A, indicating that the high affinity of Man-Au NCs toward Con A was ascribed to the high mannose loading on their surface. Compared to free mannose, the association constant value K of NH_2-Man-Au NCs to Con A was increased by 62 times, while the K value of Man-Au NCs to Con A was increased by nearly 1300 times. These results showed that the affinity between carbohydrate and protein was greatly enhanced due to the unique multivalent effect of G-NPs. Notably, Man-Au NCs showed 21 times stronger binding affinity to Con A than NH_2-Man-Au NCs, even if the two above G-NPs having the similar mannose loading amount. This result could be attributed to the greater structural rigidity and steric hindrance of the benzene ring in NH_2-Man. In contrast, the synthesized MPTA in this work is a flexible chain, which eliminates the steric hindrance and is more conducive for carbohydrate-protein interactions. Furthermore, replacing GMBS with other similar bifunctional

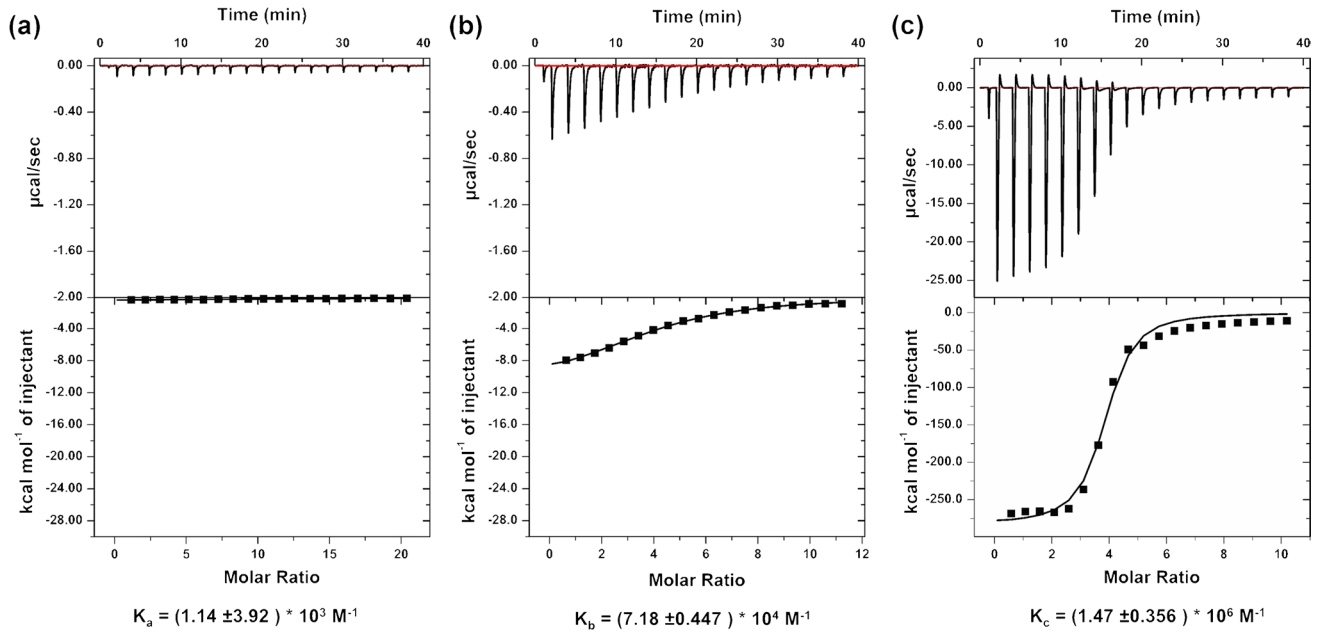

Fig. 3 ITC graphs of Con A titrations with **a** free mannose, **b** NH_2-Man-Au NCs, and **c** Man-Au NCs. The experimental data (solid squares) were fit to theoretical titration curves (solid lines) using the software supplied by the ITC manufacturer

linkers with different lengths and hydrophobicity/hydrophilicity could customize an optimal carbohydrate immobilization method for different needs in future work.

MDA-MB-231 cell imaging by Man-Au NCs

Previous reports have indicated that mannose functionalized nanoparticles could specifically target cancer cells with overexpressed mannose receptors (MRs) [33]. To further verify the potentiality of the as-prepared G-NPs' application in cancer cell targeting imaging or therapy, human breast cancer MDA-MB-231 cells with high expression of MRs were selected as the model to perform the cell imaging using Man-Au NCs. Firstly, the cell cytotoxicity of Man-Au NCs was evaluated by CCK-8 assays. As shown in Fig. S19, the cell viability was almost undisturbed after being treated with different concentrations of Man-Au NCs, demonstrating a low toxicity and good biocompatibility of Man-Au NCs for living cells [34]. Figure 4 displays the results of cell imaging with bright field, fluorescence, and merged images detected by laser scanning confocal microscopy. As shown in Fig. 4a, cells incubated with PBS displayed no fluorescence, excluding the possibility of cellular auto-fluorescence. When cells were incubated with GSH-Au NCs for 1.5 h, a very weak fluorescence was observed, indicating that GSH-Au NCs without mannose targeting could not be efficiently endocytosed by MDA-MB-231 cells over a short period of time (Fig. 4b). In contrast, after incubated with Man-Au NCs for 1.5 h, bright orange fluorescence of the cells was observed, which was mainly distributed in cytoplasm region, demonstrating the successful staining of MDA-MB-231 cells by Man-Au NCs within 1.5 h (Fig. 4c). The rapid cell imaging was attributed to the specific recognition between the Man-Au NCs and the overexpressed MRs on the surface of MDA-MB-231 cells. To further confirm the specific targeting ability of Man-Au NCs for human breast cancer cells, 3T3 cells, a kind of normal cell which shows poor MR expression was selected as negative control. As shown in Fig. S20, no obvious fluorescence signal could be observed from 3T3 cells incubated with Man-Au NCs under the same experiment conditions. These findings further validated that the G-NPs prepared with MPTA were good candidates for cancer cells imaging based on the carbohydrate-protein interaction. In addition, this Au NC-based fluorescent glycoprobe shows good optical properties, easy functionalization, and good biocompatibility, which make it hold great application potential in subsequent tumor therapy [35].

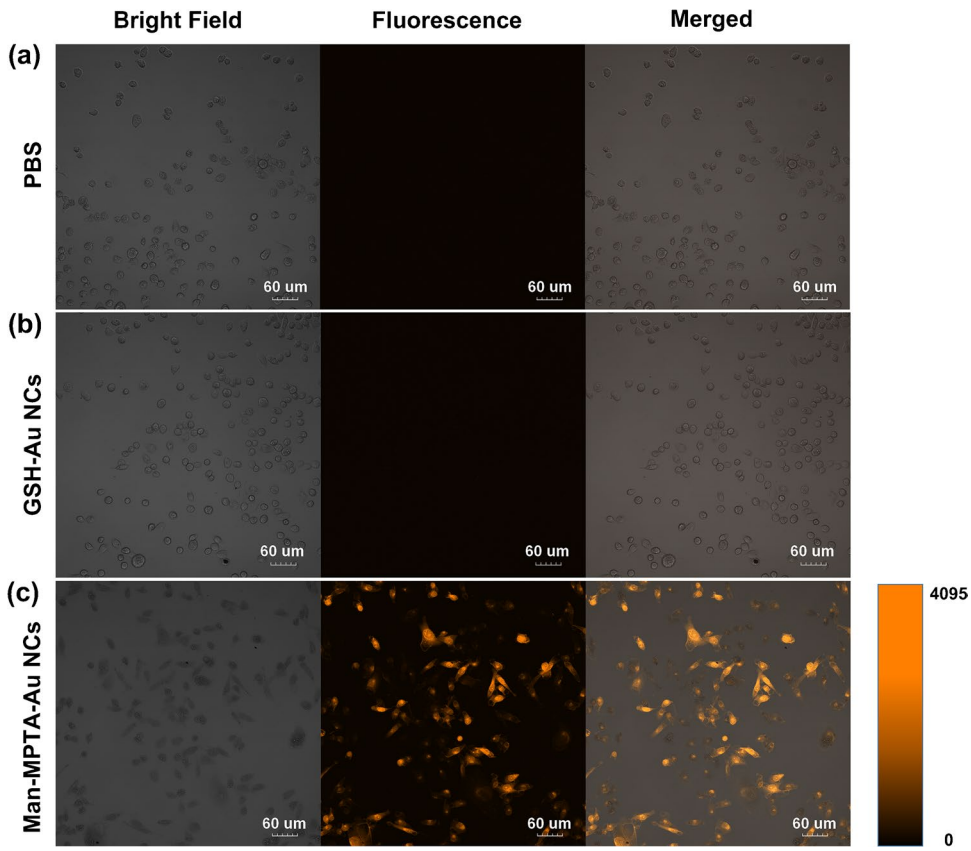

Fig. 4 Confocal fluorescence images of MDA-MB-231 cells after incubated with PBS (10 mM, pH 7.4), GSH-Au NCs, and ManMPTA-Au NCs for 1.5 h (Ex: 405 nm). Scale bar: 60 μm

Conclusion

This work presented the synthesis of a new bifunctional linker MPTA and a novel strategy for preparing G-NPs based on it. Through a chemo- and stereo-selective reducing end ring-closure reaction with MPTA, any kind of reducing carbohydrates could be easily immobilized onto GSH-Au NCs under mild conditions. Meanwhile, the structure integrity of the carbohydrate was preserved well after coupling with MPTA. Taking mannose as an example, the obtained carbohydrate-conjugated GSH-Au NCs (G-NPs) exhibited good monodispersity and strong fluorescence emission. Carbohydrates modified on GSH-Au NCs still maintained their specific recognition ability for receptor proteins. More importantly, benefiting from the excellent multivalent effect of G-NPs as well as the high coupling efficiency and suitable structure of MPTA, the affinity between G-NPs and proteins was greatly enhanced compared with not only the free carbohydrates but also the G-NPs prepared from commercially available NH_2-Man. Besides, lectin sensing and cancer cell imaging were also achieved by using the fluorescent G-NPs prepared by the strategy developed in this work. In general, a new, efficient, and versatile method for G-NP preparation has been developed and can be further expanded to other nanomaterials with good performance for carbohydrate-based biosensing, bioimaging, vaccine preparation, and tumor targeted therapy, thereby becoming a robust tool in analytical chemistry and biomedical research.

Supplementary Information The online version contains supplementary material available at https://doi.org/10.1007/s00604-022-05220-w.

Funding The authors were supported by the National Natural Science Foundation of China (Grant No. 81827901) and the Fundamental Research Funds for the Central Universities (2017KFYXJJ161).

Declarations

Conflict of interest The authors declare no competing interests.

References

1. Dwek RA (1996) Glycobiology: toward understanding the function of sugars. Chem Rev 96(2):683–720
2. Crocker PR, Paulson JC, Varki A (2007) Siglecs and their roles in the immune system. Nat Rev Immunol 7(4):255–266
3. Ohtsubo K, Marth JD (2006) Glycosylation in cellular mechanisms of health and disease. Cell 126(5):855–867
4. Cipolla L, Peri F (2011) Carbohydrate-based bioactive compounds for medicinal chemistry applications. Mini-Rev Med Chem 11(1):39–54
5. Aljohani S, Hussein WM, Toth I, Simerska P (2019) Carbohydrates in vaccine development. Curr Drug Deliv 16(7):609–617
6. Lee YC, Lee RT (1995) Carbohydrate-protein interactions: basis of glycobiology. Acc Chem Res 28(8):321–327
7. de la Fuente JM, Barrientos AG, Rojas TC, Rojo J, Cañada J, Fernández A, Penadés S (2001) Gold glyconanoparticles as water-soluble polyvalent models to study carbohydrate interactions. Angew Chem Int Ed 40(12):2257–2261
8. Wang X, Ramstrom O, Yan M (2010) Quantitative analysis of multivalent ligand presentation on gold glyconanoparticles and the impact on lectin binding. Anal Chem 82(21):9082–9089
9. Wang X, Matei E, Gronenborn AM, Ramstrom O, Yan M (2012) Direct measurement of glyconanoparticles and lectin interactions by isothermal titration calorimetry. Anal Chem 84(10):4248–4252
10. Reuven EM, Leviatan Ben-Arye S, Yu H, Duchi R, Perota A, Conchon S, Bachar Abramovitch S, Soulillou JP, Galli C, Chen X, Padler-Karavani V (2019) Biomimetic glyconanoparticle vaccine for cancer immunotherapy. ACS Nano 13(3):2936–2947
11. Hu J, Wu W, Qin Y, Liu C, Wei P, Hu J, Seeberger PH, Yin J (2020) Fabrication of glyco-metal-organic frameworks for targeted interventional photodynamic/chemotherapy for hepatocellular carcinoma through percutaneous transperitoneal puncture. Adv Funct Mater 30(19):1910084
12. Marradi M, Chiodo F, Garcia I, Penades S (2013) Glyconanoparticles as multifunctional and multimodal carbohydrate systems. Chem Soc Rev 42(11):4728–4745
13. Chen X, Ramstrom O, Yan M (2014) Glyconanomaterials: emerging applications in biomedical research. Nano Res 7(10):1381–1403
14. Hao N, Neranon K, Ramstrom O, Yan M (2016) Glyconanomaterials for biosensing applications. Biosens Bioelectron 76:113–130
15. Morelli L, Polito L, Richichi B, Compostella F (2021) Glyconanoparticles as tools to prevent antimicrobial resistance. Glycoconjugate J 38:475–490
16. Yu K, Hai X, Yue S, Song W, Bi S (2021) Glutathione-activated DNA-Au nanomachine as targeted drug delivery platform for imaging-guided combinational cancer therapy. Chem Eng J 419:129535
17. Yue S, Li Y, Qiao Z, Song W, Bi S (2021) Rolling circle replication for biosensing, bioimaging, and biomedicine. Trends Biotechnol 39(11):1160–1172
18. Qiao Z, Zhang J, Hai X, Yan Y, Song W, Bi S (2021) Recent advances in templated synthesis of metal nanoclusters and their applications in biosensing, bioimaging and theranostics. Biosens Bioelectron 176:112898
19. Wang X, Ramstrom O, Yan M (2010) Glyconanomaterials: synthesis, characterization, and ligand presentation. Adv Mater 22(17):1946–1953
20. O'Neil CL, Stine KJ, Demchenko AV (2018) Immobilization of glycans on solid surfaces for application in glycomics. J Carbohydr Chem 37(4):225–249
21. Villadsen K, Martos-Maldonado MC, Jensen KJ, Thygesen MB (2017) Chemoselective reactions for the synthesis of glycoconjugates from unprotected carbohydrates. Chem Bio Chem 18(7):574–612
22. Wei M, McKitrick TR, Mehta AY, Gao C, Jia N, McQuillan AM, Heimburg-Molinaro J, Sun L, Cummings RD (2019) Novel reversible fluorescent glycan linker for functional glycomics. Bioconjug Chem 30(11):2897–2908
23. Wang X, Liu LH, Ramstrom O, Yan M (2009) Engineering nanomaterial surfaces for biomedical applications. Exp Biol Med 234(10):1128–1139
24. Liu LH, Dietsch H, Schurtenberger P, Yan M (2009) Photoinitiated coupling of unmodified monosaccharides to iron oxide nanoparticles for sensing proteins and bacteria. Bioconjug Chem 20(7):1349–1355

25. Jayawardena HS, Wang X, Yan M (2013) Classification of lectins by pattern recognition using glyconanoparticles. Anal Chem 85(21):10277–10281
26. Zhang J, Kováč P (1999) Studies on vaccines against cholera. Synthesis of neoglycoconjugates from the hexasaccharide determinant of Vibriocholerae O: 1, serotype Ogawa, by single-point attachment or by attachment of the hapten in the form of clusters. Carbohydr Res 321(3-4):157–167
27. Munneke S, Prevost JR, Painter GF, Stocker BL, Timmer MS (2015) The rapid and facile synthesis of oxyamine linkers for the preparation of hydrolytically stable glycoconjugates. Org Lett 17(3):624–627
28. Peri F, Dumy P, Mutter M (1998) Chemo-and stereoselective glycosylation of hydroxylamino derivatives: a versatile approach to glycoconjugates. Tetrahedron 54(40):12269–12278
29. Munneke S, Dangerfield EM, Stocker BL, Timmer MSM (2017) The versatility of N-alkyl-methoxyamine bi-functional linkers for the preparation of glycoconjugates. Glycoconj J 34(5):633–642
30. Munneke S, Hill JC, Timmer MSM, Stocker BL (2017) Synthesis and hydrolytic stability of N- and O-methyloxyamine linkers for the synthesis of glycoconjugates synthesis and hydrolytic stability of N- and O-methyloxyamine linkers for the synthesis of glycoconjugates. Eur J Org Chem 2017(25):3722–3728
31. Luo Z, Yuan X, Yu Y, Zhang Q, Leong DT, Lee JY, Xie J (2012) From aggregation-induced emission of Au(I)-thiolate complexes to ultrabright Au(0)@Au(I)-thiolate core-shell nanoclusters. J Am Chem Soc 134(40):16662–16670
32. Sha Q, Guan R, Su H, Zhang L, Liu B-F, Hu Z, Liu X (2020) Carbohydrate-protein template synthesized high mannose loading gold nanoclusters: a powerful fluorescence probe for sensitive Concanavalin A detection and specific breast cancer cell imaging. Talanta 218:121130
33. Gary-Bobo M, Mir Y, Rouxel C, Brevet D, Basile I, Maynadier M, Vaillant O, Mongin O, Blanchard-Desce M, Morère A, Garcia M, Durand JO, Raehm L (2011) Mannose-functionalized mesoporous silica nanoparticles for efficient two-photon photodynamic therapy of solid tumors. Angew Chem Int Ed 50(48):11425–11429
34. Zhang XD, Wu D, Shen X, Liu PX, Fan FY, Fan SJ (2012) In vivo renal clearance, biodistribution, toxicity of gold nanoclusters. Biomaterials 33(18):4628–4638
35. Khan H, Mirzaei HR, Amiri A, Kupeli Akkol E, Ashhad Halimi SM, Mirzaei H (2021) Glyco-nanoparticles: new drug delivery systems in cancer therapy. Semin Cancer Biol 69:24–42